Tanzania Journal of Science 50(3): 555-568, 2024
ISSN 0856-1761, e-ISSN 2507-7961

Performance of a Bipolar Output Voltage DC-DC Converter for Voltage Regulation for Solar PV System Application

Stampinus M. Stephano[1,2*], Jackson. J. Justo[2], and Bakari M. M. Mwinyiwiwa[2]
[1]*Department of Agricultural Engineering, Sokoine University of Agriculture, P. O. Box 3003, Morogoro, Tanzania*
[2]*Department of Electrical Engineering, University of Dar es Salaam, P. O. Box 35131, Dar es Salaam, Tanzania*
Email addresses: jackjusto2009@gmail.com, bakari1mwinyiwiwa@gmail.com
[*]*Corresponding author: Email: stampkazimili@gmail.com/stampinus.stephano@sua.ac.tz.*
Received 4 March 2024, Revised 20 June, Accepted 15 September, Published 30 Sept. 2024
https://dx.doi.org/10.4314/tjs.v50i3.11

Abstract

A combined Single-Ended Primary-Inductor Converter (SEPIC) and Cuk DC-DC converter that provides a bipolar outputs voltage at the DC bus is widely used in applications especially solar photovoltaic (SPV) system. Maintaining constant output voltages at the DC bus under variable loads and input voltage from SPV is of great interest to many researchers. This paper presents a 400 W mathematical model of a combined SEPIC and Cuk DC-DC converter through state space averaging (SSA) in a continuous conduction mode (CCM). A nested voltage and current control loops are used to regulate voltage and increase the performance of the converter. These controls use Proportional-Integral (PI) controllers to track the desired input reference signal and eliminate any disturbance from the load. The entire model with its control algorithm was modelled in MATLAB/Simulink environment and validation results to evaluate its performance are presented. The controller was able to maintain required bus voltage of 24 V DC and -/+12 V at the output DC bus. DC bus voltage regulation was tested at varying input voltages and varying loads connected at the output, where, in all those scenarios, the converter could regulate its output voltage to required value.

Keywords: Solar PV systems; Bipolar output DC voltage; Voltage regulation; Nested PI controllers

Introduction

Being clean, reliable and emission-free, solar photovoltaic (SPV) source is considered as one of the most promising renewable energy sources. The output voltage and power from solar PV panels depend on the solar irradiance, temperature and partial shading of the particular area (Justo and Mushi 2020; Zhang et al. 2011). Thus, DC output voltage of (SPV) module is not constant, however, most of DC loads require constant voltage. Therefore, SPV systems are integrated with controlled DC-DC converters to provide constant output voltages to loads from varying output voltage of SPV modules (Gupta and Garg 2017, Justo et al. 2013). Conventional DC-DC converters have been facing different problems such as primary loss and high voltage stresses in their switching devices. Moreover, conventional converters require high rated design equipment when required in handling large power (Arunkumari and Indragandhi 2017; Cao et al. 2017; Torkan and Ehsani 2018). Also, the DC output voltages from most of convectional power converters are unipolar, thus, are limited when it comes to inverter pairing options and multi-voltage applications. Sometimes, these conventional power converters typically lead to leakage currents and complexity when required to produce bipolar DC output voltage (Li et al.

2015, Ozkan and Hava 2012). That may lead to an increased running cost of SPV systems and their integration applications.

DC-DC power converters range from isolated to non-isolated DC-DC power converters. Although, attention has been paid on isolated high-step converter, but they have been confronted with high switching stresses and low efficiency. This introduces barriers when using isolated DC-DC converters (Evran and Aydemir 2014; Li et al. 2012; Park et al. 2012). Non-Isolated DC-DC power converters include buck and boost power converters that give the output voltage less than and greater than the input voltage, respectively. The two configurations have few components making them easier to control and implement. However, these converters suffer from having limited range of output voltages and hence they have low efficiency (Vekhande and Fernandes 2012). Another type of power converter is the buck-boost which is able to generate an inverted output voltage greater than or less than the input with ungrounded power switch (Muhammad et al. 2014). This requires a complex sensing and feedback circuit such as an inverting Op-Amp is needed for the closed looped feedback control that leads to poor performance when used for high gain application. Moreover, in this converter, the input current and charging current of output capacitor is discontinuous causing high voltage stresses to the switch that results in large size of filters (Durán et al. 2008; Pradhan and Panda 2018). Cuk and SEPIC converter has the same voltage ratio and polarity as buck-boost converter with the difference that they have two inductors. Also, Cuk and SEPIC converters have continuous input current that eliminates the use of large decoupling capacitors between SPVs and the input of Cuk converter. Unlike buck-boost converter, power switching device is ground-referenced allowing the use of simple and cheap gate driver (Ferrera et al. 2015; Mwinyiwiwa 2016). Moreover, those converters can operate in combination or cascading more than one converter. Therefore, Cuk and SEPIC DC-DC converters in their combination are of great concern in this paper.

DC-DC converters are integrated with control circuits or controllers so as to provide constant or fixed output DC voltage to the load from a varying SPV source (Dileep and Singh 2017, Taghvaee et al. 2013). There are different DC-DC Converters control techniques in which control techniques with simple and robust design, low cost and good performance at any circumstances are a great deal of interest (Bajoria et al. 2017). Some of these controllers' voltage and current mode control that adapt PI controllers for their numerical methods algorithm. The other type is predictive control that achieves excellent control strategy; however, it lies in the necessity to develop accurate mathematical model for the control system. There are also other artificial intelligence methods such as fuzzy logic control, artificial neural networks, sliding mode control and hysteretic control (Chen et al. 2023; Lešo et al. 2018; Ma et al. 2020). For the purpose of this research, traditional PI controller has been selected for the voltage and current mode control of the proposed converter as it is easy to design, robust, cheaper for industrial application and easy to set parameters.

In this paper a 400 W SEPIC and Cuk DC-DC converter equipped together with PI controllers for SPV applications is proposed. The converter aimed at producing constant bipolar output DC voltages of 12 V and 24 V at the DC bus from a varying 12 V solar PV system source. The PI controller was modelled and its performance with its converter is validated using MATLAB/Simulink software. This is the main motive behind this paper. This paper describes the proposed combined Cuk and SEPIC DC-DC converter and step to step art of mathematical modelling of a nested (cascaded) voltage and current control modes with PI controller.

The rest of the paper is organized as follows: Section II highlights the description and mathematical modelling of the proposed DC-DC converter. Section III describes the detailed design and mathematical modelling of the control algorithms for the proposed converter. Meanwhile, system parameters and extensive simulation studies together with simulation results and discussion on performance evaluation are presented in Section IV. Section V draws the main conclusion of the paper.

Methods

Descriptions of proposed Combined SEPIC and Cuk DC-DC converter

The proposed DC-DC converter comprises of a combination of two converters namely Cuk and SEPIC DC-DC converters as shown in Figure 1, where L_{in} is the input inductor, L_1 and L_2 are Cuk and SEPIC transfer inductors respectively, C_1 and C_2 are Cuk and SEPIC input capacitors and Co_1 and Co_2 are output capacitors. D_1 and D_2 are diodes and S is the switching device. Cuk converter produces a negative polarity output voltage with respect to the positive polarity input voltage, whereas SEPIC converter produces a positive polarity output voltage. The combination of these converter holds due to the following reasons stated in the research of (Anand and Singh 2018) and in researches of (Ferrera et al. 2015; Ghosh et al. 2020; Litrán et al. 2020; Nathan et al. 2019);

- Cuk and SEPIC converters have continuous input currents and can both step-up and step-down voltages.
- Both Cuk and SEPIC converters have same voltage conversion ratios with opposite polarities, hence they can be combined and share the same ground and switch that simplifies the implementation of the control strategies.
- Cuk and SEPIC converters exhibit non-pulsating input currents, but Cuk converter exhibit non-pulsating output current and SEPIC exhibit pulsating output current. This suggests the combination of these two converters at the same switching node.
- Cuk and SEPIC structures are very versatile allowing to implement isolated and bidirectional versions.
- These two converters have the same input structures and have the same number of components.
- The combined converter uses a single switch configuration that helps to reduce switching stresses across the device due to available common mid-point.

Mathematical modelling of the Combined SEPIC and Cuk DC-DC converter

The proposed DC-DC converter is analyzed in continuous conduction mode such that the input and output inductors are designed to operate in a continuous inductor current mode and output capacitors are designed such that voltages across them should remain continuous throughout the switching period. When the switch is ON to a period time of dT, capacitors are charging and inductor currents are decaying and verse vise to a period time of $(1\text{-}d)T$ when the switch is OFF (T is the periodic time and d is the duty cycle of the switch). The whole process is mathematically analyzed as in (1) through (3) at the period when the switch is ON and in (4) to (5) at the period when the switch is OFF.

$$\begin{cases} di_{L_{in}}/dt = v_S/L_{in} \\ di_{L_1}/dt = v_{C_1}/L_1 \\ di_{L_2}/dt = \left(v_{C_2} - v_{O_2}\right)/L_2 \end{cases} \quad (1)$$

$$\begin{cases} dv_{C_1}/dt = -i_{L_1}/C_1 \\ dv_{C_2}/dt = -i_{L_2}/C_2 \\ dv_{C_{O_1}}/dt = -v_{O_1}/C_{O_1}R_1 \\ dv_{C_{O_2}}/dt = 1/C_{O_2}\left(i_{L_2} - v_{O_2}/R_2\right) \end{cases} \quad (2)$$

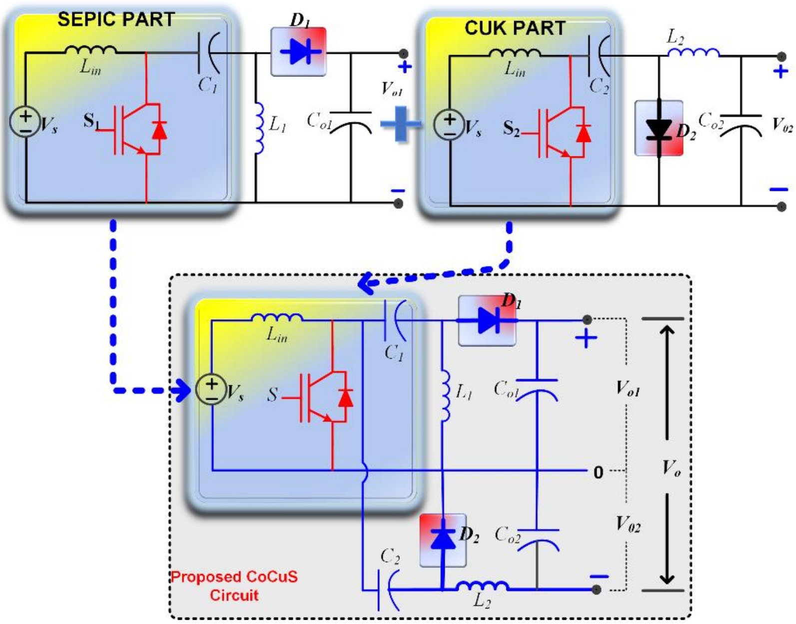

Figure 1: Formulation of the proposed DC-DC converter.

$$\begin{cases} i_{D_1} = \dfrac{i_{L_{in}}}{2} + i_{L_1} \\ i_{D_2} = \dfrac{i_{L_{in}}}{2} + i_{L_2} \end{cases} \quad (3)$$

$$\begin{cases} \dfrac{di_{L_{in}}}{dt} = \dfrac{v_S - v_{C_1} - v_{O_1}}{L_{in}} \\ \dfrac{di_{L_1}}{dt} = \dfrac{-v_{O_1}}{L_1} \\ \dfrac{di_{L_2}}{dt} = \dfrac{-v_{O_2}}{L_2} \end{cases} \quad (4)$$

$$\begin{cases} dv_{C_1}/dt = i_{L_{in}}/2C_1 \\ dv_{C_2}/dt = i_{L_{in}}/2C_2 \\ dv_{C_{O_1}}/dt = 1/C_{O_1}\left(i_{L_{in}} + i_{L_1} - \left(-v_{O_1}\right)/R_1\right) \\ dv_{C_{O_2}}/dt = 1/C_{O_2}\left(i_{L_2} - v_{O_2}/R_2\right) \end{cases} \quad (5)$$

Under steady state operation assuming ideal and lossless components and ignoring higher ripples of the components, the parametric values of the converter's components are determined using (6) to (12). Converter's specification in Converter's specification in Table 1 give the parametric values of the components as they are shown in Table 2.

$$L_{in} = \frac{V_{S_{max}}^2 \times V_O}{\left(V_{S_{max}} + V_O\right) \times P_O \left(\dfrac{\Delta I_{L_{in}}}{I_{L_{in}}}\right) f_{sw}} \quad (6)$$

$$L_1 = \frac{2V_{S_{max}} \times V_O^2}{\left(V_{S_{max}} + V_O\right) \times P_O \left(\dfrac{\Delta I_{L_1}}{I_{L_1}}\right) f_{sw}} \quad (7)$$

$$L_2 = \frac{2V_{S_{max}} \times V_O^2}{\left(V_{S_{max}} + V_O\right) \times P_O \left(\dfrac{\Delta I_{L_2}}{I_{L_2}}\right) f_{sw}} \quad (8)$$

$$C_1 = \frac{P_O}{2V_{S_{min}}\left(V_{S_{min}} + V_O\right) \times \left(\dfrac{\Delta v_{C_1}}{v_{C_1}}\right) f_{sw}} \quad (9)$$

$$C_2 = \frac{P_O}{2\left(V_{S_{min}} + V_O\right)^2 \times \left(\dfrac{\Delta v_{C_2}}{v_{C_2}}\right) f_{sw}} \quad (10)$$

$$C_{O_1} = \frac{P_O}{2V_O\left(V_{S_{min}} + V_O\right) \times \left(\dfrac{\Delta v_{C_{O_1}}}{v_{C_{O_1}}}\right) f_{sw}} \quad (11)$$

$$C_{O_2} = \frac{P_O}{16V_O^2 \left(\dfrac{\Delta v_{C_{O_2}}}{v_{C_{O_2}}}\right) f_{sw}} \quad (12)$$

Table 1: Design specifications for proposed converter

Parameter	Values
Input voltage range (V_{Smin} to V_{Smax})	9.8 to 17.0 V
Nominal output voltage (V_o)	+/- 12 V
Output power (P_o)	400.0 W
Input and output current ripples ($\Delta I_L/I_L$)	0.05
Input voltage ripple ($\Delta V/V_C$)	0.08
Output voltage ripple ($\Delta v_{co}/v_{co}$)	0.02
Switching frequency (f_{sw})	50 kHz

Moreover, the proposed converter is modelled using state space averaged (SSA) to have time depended variables x known as small signal variables or perturbed variables represented with cap (^). Therefore, by applying SSA and small signal perturb methods to dynamic and steady state equations of the two operating states of the converter, the new mathematical model of the converter is given as in (13);

Table 2: DC-DC converter simulation parameters

Parts/Parameters	Designed Values
L_{in}, L_1, L_2	119.6 µH, 169 µH, 169 µH
C_1, C_2, C_{o1}, C_{o2}	234 µF, 78 µF, 765 µF, 8.68 µF

$$\dot{x}(t) = Ax + B\hat{v}_S + C\hat{d} \qquad (13)$$

in which the variables of x are such that;

$$x = \begin{bmatrix} \hat{i}_{L_{in}} & \hat{i}_{L_{in}} & \hat{i}_{L_1} & \hat{i}_{L_2} & \hat{v}_{C_1} & \hat{v}_{C_2} & \hat{v}_{O_1} & \hat{v}_{O_2} \end{bmatrix}^T$$

and A, B and C are matrices that are expressed in as; -

$$B = \begin{bmatrix} \frac{1}{L_{in}} & \frac{1}{L_{in}} & 0 & 0 & 0 & 0 & 0 & 0 \end{bmatrix}^T$$

$$C = \begin{bmatrix} \frac{V_{C_2}}{L_{in}} & \frac{V_{C_1}+V_{O_1}}{L_{in}} & \frac{V_{C_1}+V_{O_1}}{L_1} & \frac{V_{C_2}}{L_2} & \frac{I_{L_{in}}+2I_{L_1}}{2C_1} & \frac{I_{L_{in}}+2I_{L_2}}{2C_2} & \frac{1}{C_{O_1}}\left(I_{L_{in}}+I_{L_1}\right) & 0 \end{bmatrix}^T$$

$$A = \begin{bmatrix} 0 & 0 & 0 & 0 & 0 & 0 & -\left(\frac{1-D}{L_{in}}\right) & 0 \\ 0 & 0 & 0 & 0 & -\left(\frac{1-D}{L_{in}}\right) & 0 & -\left(\frac{1-D}{L_{in}}\right) & 0 \\ 0 & 0 & 0 & 0 & \frac{D}{L_1} & 0 & -\left(\frac{1-D}{L_1}\right) & 0 \\ 0 & 0 & 0 & 0 & 0 & \frac{D}{L_2} & 0 & \frac{1}{L_2} \\ \frac{1-D}{2C_1} & -\frac{D}{C_1} & 0 & 0 & 0 & 0 & 0 & 0 \\ \frac{1-D}{2C_2} & 0 & -\frac{D}{C_2} & 0 & 0 & 0 & 0 & 0 \\ \frac{1-D}{C_{O_1}} & \frac{1-D}{C_{O_1}} & 0 & 0 & 0 & 0 & \frac{1}{C_{O_2}R_2} & 0 \\ 0 & 0 & \frac{1}{C_{O_2}} & 0 & 0 & 0 & 0 & \frac{1}{C_{O_2}R_2} \end{bmatrix}$$

Controller Design for Proposed DC-DC Converter

The key point in the control scheme is to maintain the constant output voltages at the best performance of the converter. In this design, the following considerations are considered as:

- Switching device and diodes are considered ideal.
- The system is operating in CCM
- Very small input and output ripples are considered
- All internal resistances of passive elements are neglected

As shown in Figure 2 the control structure comprises a nested control loop (voltage and current control loops). The current control decouples the current inductor control from that of the capacitor voltage control. Therefore, the current loop controls inductor current against any variations of parameters which increases the versatility of control scheme. The design is in such a way that inner loop (current control) is faster than the outer loop (voltage control). In both control loops, PI controller is used to track the desired reference input signals with reference to the measured signal and control duty cycle to the converter is provided by inner loop. The general transfer function of the PI controller in closed loop is given as (14) (Ogata 2010)

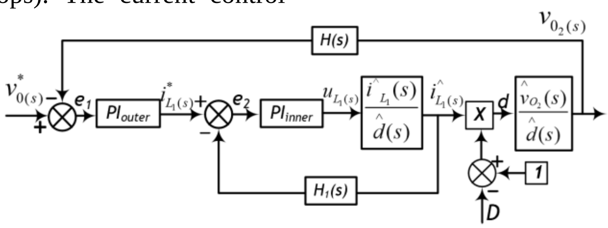

Figure 2: A nested voltage and current control. loops.

$$G(s) = K_p + \frac{K_i}{s} \begin{cases} K_p > 0 \\ K_i > 0 \end{cases} \qquad (14)$$

Outer Voltage control loop

Consider the Figure 3 below representing the voltage control, the identical block *I* is used as inner control loop. If the output voltage is not dynamic, then, the feedback transfer function, *H(s)* = 1.

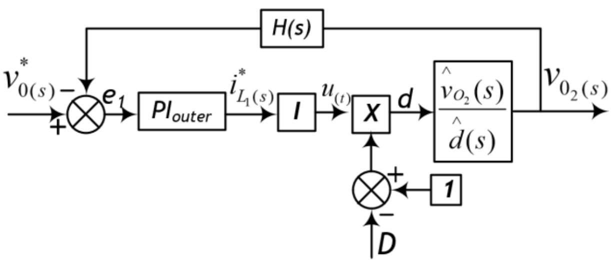

Figure 3: Outer voltage control loop.

Thus, using (13), the final transfer function from inner loop to output voltage ($v_{co2}(s)/d(s)$) is given as (15), where, y_i and x_i are constants in which their values depends on converters' passive elements values, steady state duty ratio and passive component voltage ratings. The resulting transfer function is the 4th order system, then the PI controller is tuned using Ziegler-Nichols approach as in (Bajoria et al. 2017; Ogata 2010; Rabiaa et al. 2019) to have a final closed loop function ($H_{outer}(s)$) of outer control loop as expressed in (16). The PI values are 0.0001 and 20 respectively.

$$\frac{\hat{v}_{O_2}(s)}{\hat{d}(s)} = \frac{\sum_{i=1}^{n=3} y_i s^i}{\sum_{i=1}^{n=4} x_i s^i + 1} \quad (15)$$

$$H_{outer}(s) = \frac{\sum_{j=1;k=1}^{n;m=3} x_{j(2)} s^k + Q_N}{\sum_{i=1;l=1}^{N;M=5} y_{i(2)} s^l - Q_N} \quad (16)$$

where; x and y are constant parameters that depend on power converter's passive component values and Q_N is equal to 1560.

Inner Current control loop

Using the same procedures applied for voltage control loop and considering Figure 4 the transfer function for current control loop is given as in (17) below.

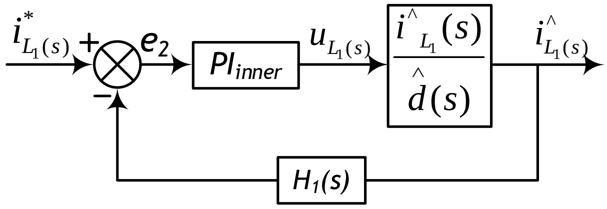

Figure 4: Inner current control loop.

$$\frac{\hat{i}_{L_1}(s)}{\hat{d}(s)} = \frac{\beta_1 c_1 + \delta_1 a_1}{\alpha_1 a_1 - \beta_1 b_1} \quad (17)$$

where:

$$\alpha_1 = s + \frac{D^2}{C_1 L_1 s} + \frac{(1-D)^2}{C_{O_1} L_1 s + \frac{L_1}{R_1}}$$

$$\beta_1 = \frac{D(1-D)}{2C_1 L_1 s} + \frac{(1-D)^2}{C_{O_1} L_1 s + \frac{L_1}{R_1}}$$

$$\delta_1 = \frac{(1-D)\left(I_{L_{in}} + I_{L_1}\right)}{C_{O_1} L_1 s + \frac{L_1}{R_1}} - \frac{D\left(I_{L_{in}} + 2I_{L_1}\right)}{2C_1 L_1 s}$$

$$a_1 = s + \frac{(1-D)^2}{2C_1 L_{in} s} + \frac{(1-D)^2}{C_{O_1} L_{in} s + \frac{L_{in}}{R_1}}$$

$$b_1 = s + \frac{D(1-D)}{C_1 L_{in} s} + \frac{(1-D)^2}{C_{O_1} L_{in} s + \frac{L_{in}}{R_1}}$$

$$c_1 = \frac{(1-D)\left(I_{L_{in}} + I_{L_1}\right)}{2C_1 L_{in} s} - \frac{(1-D)\left(I_{L_{in}} + I_{L_1}\right)}{C_{O_1} L_{in} s + \frac{L_{in}}{R_1}} + \frac{\left(V_{C_1} + V_{O_1}\right)}{L_{in}}$$

Again, the resulting transfer function is of higher order system, therefore with proper tuning of PI controller parameters which are 0.0064 and 32.5, the final inner loop closed transfer function ($H_{inner}(s)$) is given as (18) where; x and y are constant parameters that depend on power converter's passive component values and Q_D is equal to 20000.

$$H_{inner}(s) = \frac{\sum_{j=1;k=1}^{n;m=5} x_{j(2)} s^k + Q_D}{\sum_{i=1;l=1}^{N;M=7} y_{i(2)} s^l + Q_D} \quad (18)$$

Results, Performance Validation and Discussions

The proposed model and its control strategy as in Figure 5 was modelled in MATLAB/Simulink. The performance of the proposed DC-DC converter is validated under two scenarios as explained in sub-sections below, where, the first scenario is under varying DC output load and the second scenario is under varying input voltage from SPV.

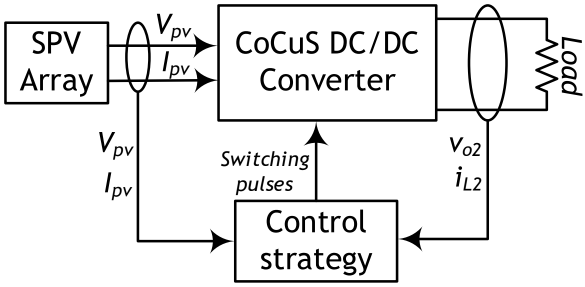

Figure 5: Proposed model of CoCuS DC/DC converter and control strategy.

Converter's performance under load variations

Under load variations, the converter was first operated to supply a constant load of 100 W at a constant input nominal DC voltage of 12 V from SPV system. Then, the load was gradually added to the converter at the period of 0.35 sec, 0.6 sec where the load was increased to 160 W and 200 W respectively as shown in Figure 6. Regardless the changes in DC loads connected to the converter, the proposed converter was capable of maintaining the constant DC output voltages. As shown in Figure 7 and Figure 8, the converter is capable of providing constant 12 V voltage on both positive and negative terminals. Moreover, the converter is able to produce constant 24 V DC voltage at the positive and negative terminals of the converter.

Converter's performance under input voltage variations

Since the output voltage from SPV system stochastic, therefore, the performance of the converter was also observed under varying input voltages. As shown in Figure 9 and Figure 10, the proposed converter could manage to maintain constant output voltages of +12 V to constant -12 V at the DC bus. In this case, the solar irradiance was varied from 900 W/m^2 to 1150 W/m^2 and gradually decreased to 700 W/m^2. In all those cases of varying insolation, also the output voltage from SPV varied too. However, as the requirement, the proposed converter could maintain the constant bipolar output voltages.

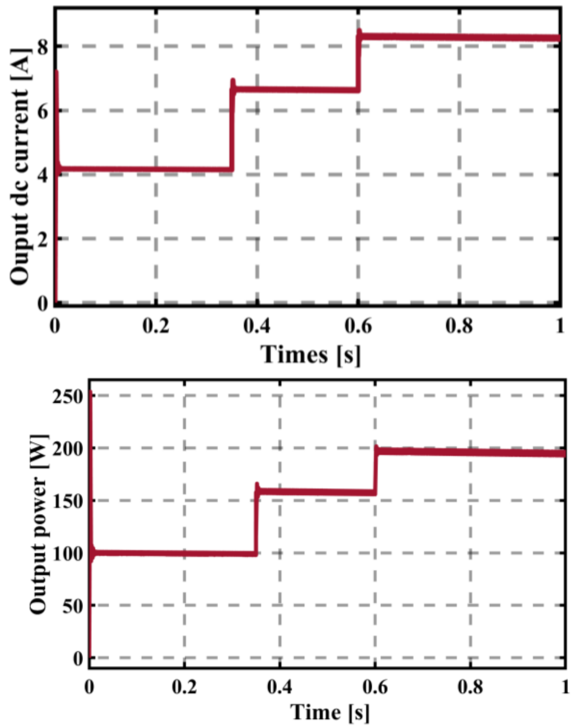

Figure 6: Load output current and power for varying DC load.

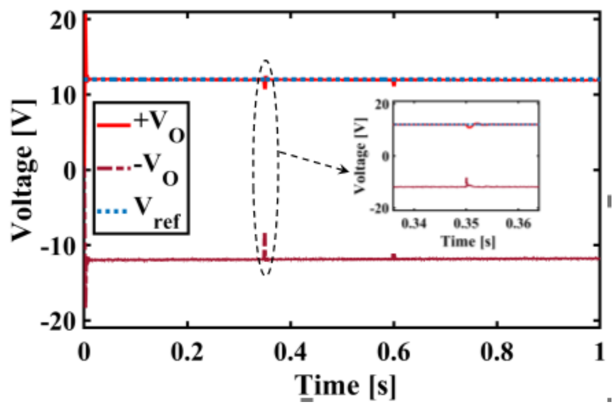

Figure 7: Bipolar positive and negative output voltage with load change.

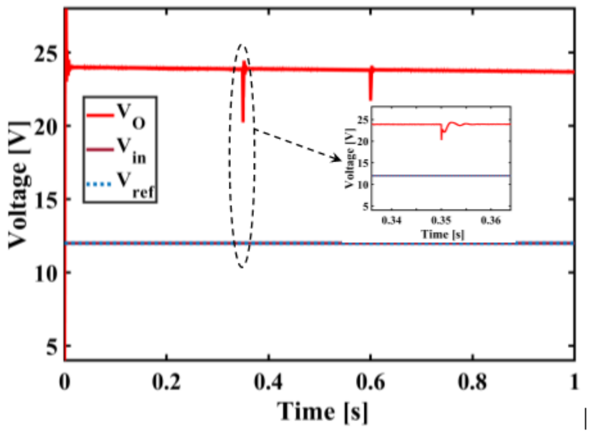

Figure 8: Terminal output load voltage with load change.

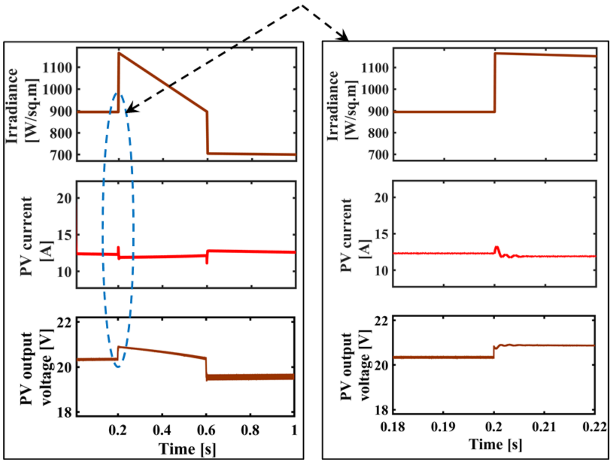

Figure 9: Solar irradiance, PV current and voltage variations.

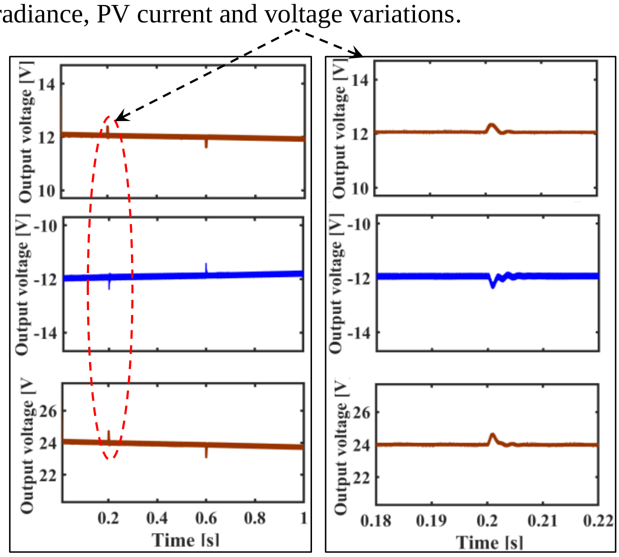

Figure 10: Output voltage of the converter at varying SPV parameters (solar irradiance).

Quantitative Comparison of the Proposed DC-DC Converter

The proposed combined SEPIC and Cuk DC-DC converter is compared with its counterpart buck-boost DC-DC converter by comparing their efficiency at different loads and voltage gain at different duty cycles.

Efficiency Comparison Analysis

Table **3** and Figure 11 show efficiency of two converters at different loads. From those results, it is shown that buck-boost converter has better efficiency at a load of 100 W, but as load increases, efficiency of buck-boost converter is poor compared to a proposed converter. Therefore, buck-boost converter shows greater performance under light loads

The efficiency of the two converters (buck-boost and proposed DC-DC converters) is determined using loss calculation methods as described in (Babaei et al. 2016; Shen et al. 2006). The efficiency (η) of buck-boost and proposed DC-DC converters is given by (19), where P_o is the output power to the load, P_{in} in the input power to the converter.

$$\eta = \frac{P_O}{P_{in}} \times 100\% \qquad (19)$$

and shows poor performance when load increases. However, the proposed combined SEPIC and Cuk DC-DC converter shows high efficiency of above 96% to all loads connected to it. This depicts advanced application of this bipolar output voltages DC-DC converter.

Table 3: Efficiency comparison under different loads

Load (W)	Efficiency (%) Buck-Boost converter	Efficiency (%) Proposed Converter
100	98.51	97.73
150	87.07	96.12
200	86.35	94.93
250	85.76	94.50
300	85.29	93.90
350	85.29	92.83

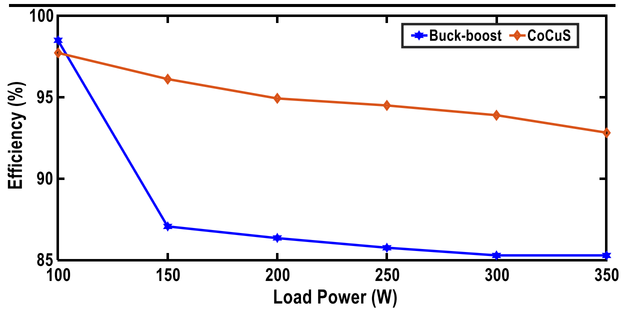

Figure 11: Efficiency curves of proposed and buck-boost DC-DC converters at different loads.

Voltage gain Comparison Analysis

Voltage gains of buck-boost and combined SEPIC and Cuk DC-DC converters are determined using (20) and (21) respectively, where d is the duty cycle, V_o is the output voltage and V_s is the input voltage. Figure 12 and Table 4 show the comparison of buck-boost and proposed DC-DC converters voltage gain at different duty cycles with constant input voltage of 12 V and DC resistive load of 300 W.

$$G_{buck-boost} = \frac{V_{O_{buck-boost}}}{V_s} = \frac{d}{1-d} \qquad (20)$$

$$G_{SEPIC-Cuk} = \frac{V_{O_{SEPIC-Cuk}}}{V_s} = 2\left(\frac{d}{1-d}\right) \qquad (21)$$

From those results, it was shown that both converters start boost operations in lower duty cycles, but the proposed converter showed a greater voltage gain compared to buck-boost converter. The voltage gain of the proposed converter was almost twice of that of the buck-boost converter.

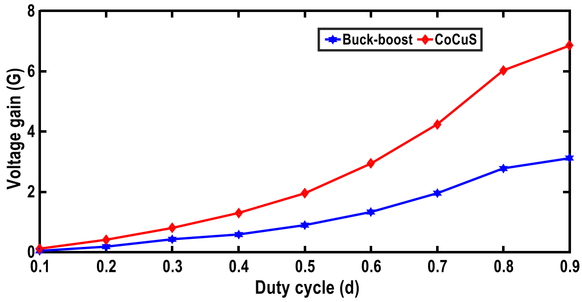

Figure 12: Simulated Voltage gain curves of proposed and buck-boost DC-DC converters at different duty cycle.

Table 4: Proposed and buck-boost converters' voltage gain at different duty cycle

Duty Cycle (*d*)	**Output Voltage (V)** Buck-Boost converter	Proposed Converter	**Voltage Gain** Buck-Boost converter	Proposed Converter
0.1	0.531	1.397	0.044	0.116
0.2	2.184	4.93	0.182	0.411
0.3	4.283	9.63	0.428	0.803
0.4	7.043	15.6	0.587	1.300
0.5	10.77	23.42	0.896	1.952
0.6	15.98	35.28	1.332	2.940
0.7	23.45	50.90	1.954	4.242
0.8	33.37	72.38	2.781	6.032
0.9	37.39	82.24	3.116	6.853

Conclusion and Recommendations

The performance of a combined Cuk and SEPIC DC-DC converter with bipolar output voltage for SPV application is discussed in this paper. The converter was able to maintain constant output voltages at varying DC loads and output PV voltage. Moreover, the performance of the proposed converter was compared with that of buck-boost DC-DC converter. The proposed converter has high efficiency above 96% and high gain compared to its counterpart buck-boost converter. The proposed converter applied the conventional commonly used PI controller to provide required signal, however, the converter parameters assumed linearity of the converter. However, the converter is not linear as it was assumed. Therefore, the future perspectives of this research focus on advanced control techniques such as mode predictive control and adaptive control for analysis the performance of the novel DC-DC converter.

Conflict of Interests:

The author declares no conflict of interest regarding this work

References

Anand A and Singh B. 2018 Power factor correction in cuk-SEPIC-based dual-output-converter-fed SRM drive. *IEEE Trans Industr. Electroni. 65*(2), 1117–1127. https://doi.org/10.1109/TIE.2017.2733482

Arunkumari T and Indragandhi V 2017 An overview of high voltage conversion ratio DC-DC converter configurations used in DC micro-grid architectures. *Renewable and Sustainable Energy Reviews*, *77*, 670–687. https://doi.org/10.1016/J.RSER.2017.04.036

Babaei E, Asl ES, Babayi MH and Laali S 2016 Developed embedded switched-Z-source inverter. *IET Power Electron.* 9(9): 1828–1841.
https://doi.org/10.1049/IET-PEL.2015.0921

Bajoria N, Sahu P, Nema RK and Nema S 2017 Overview of different control schemes used for controlling of DC-DC converters. *International Conference on Electrical Power and Energy Systems, ICEPES 2016*, 75–82. https://doi.org/10.1109/ICEPES.2016.7915909

Cao Y, Samavatian V, Kaskani K and Eshraghi H 2017 A Novel Nonisolated Ultra-High-Voltage-Gain DC-DC Converter With Low Voltage Stress. *IEEE Trans. Ind. Electron. 64*(4), 2809–2819. https://doi.org/10.1109/TIE.2016.2632681

Chen H, Lin W and He W 2023 Research on a DC–DC Converter and Its Advanced Control Strategy Applied to the Integrated Energy System of Marine Breeding Platforms. *J. Mar. Sci. Eng.* 11(3), 512. https://doi.org/10.3390/jmse11030512

Dileep G and Singh SN 2017 Selection of non-isolated DC-DC converters for solar photovoltaic system. *Renew. Sustain. Energy Rev.* 76(February), 1230–1247. https://doi.org/10.1016/j.rser.2017.03.130

Durán E, Sidrach-De-Cardona M, Galán J and Andújar JM 2008 Comparative analysis of Buck-Boost converters used to obtain I-V characteristic curves of photovoltaic modules. *PESC Record - IEEE Annual Power Electronics Specialists Conference*, 2036–2042. https://doi.org/10.1109/PESC.2008.4592243

Evran F and Aydemir MT 2014 Isolated high step-Up DC-DC converter with low voltage stress. *IEEE Transactions on Power Electronics*, *29*(7), 3591–3603. https://doi.org/10.1109/TPEL.2013.2282813

Ferrera MB, Litrán SP, Durán E and Andújar JM 2015 A Converter for Bipolar DC Link Based on SEPIC- Cuk Combination. *8993*(c). https://doi.org/10.1109/TPEL.2015.2429745

Ghosh S, Gaona D, Siwakoti Y and Long T 2020 Synchronous Combined Cuk-SEPIC Converter for Single Phase Transformerless Solar Inverter. 3225–3231.

Gupta N and Garg R 2017 Tuning of asymmetrical fuzzy logic control algorithm for SPV system connected to grid. *Int. J. Hydrogen Energy* 42(26): 16375–16385. https://doi.org/10.1016/J.IJHYDENE.2017.05.103

Justo JJ and Mushi AT 2020 Performance Analysis of Renewable Energy Resources in Rural Areas: A Case Study of Solar Energy *Tanz. J. Engrg. Technol.* 39(1): I

Justo JJ, Mwasilu F, Lee J and Jung JW 2013 AC-microgrids versus DC-microgrids with distributed energy resources: A review. *Renew. Sustain. Energy Rev.* 24: 387–405.
https://doi.org/10.1016/j.rser.2013.03.067

Lešo M, Žilková J, Biroš M and Talian P 2018 SURVEY OF CONTROL METHODS FOR DC-DC CONVERTERS. *Acta Electrotech. Inform.* 18(3): 41–46.
https://doi.org/10.15546/aeei-2018-0024

Li W, Fan L, Zhao Y, He X, Xu D and Wu, B 2012 High-step-up and high-efficiency fuel-cell power-generation system with active-clamp flyback-forward converter. *IEEE Trans. Industr. Electron.* 59(1), 599–610. https://doi.org/10.1109/TIE.2011.2130499

Li W, Gu Y, Luo H, Cui W, He X and Xia, C 2015 Topology review and derivation methodology of single-phase transformerless photovoltaic inverters for leakage current suppression. *IEEE Trans. Industr. Electron.* 62(7): 4537–4551. https://doi.org/10.1109/TIE.2015.2399278

Litrán SP, Durán E, Semião J and Barroso R S 2020 Single-switch bipolar output dc-dc converter for photovoltaic application. *Electronics (Switzerland)*, 9(7): 1–14.
https://doi.org/10.3390/electronics9071171

Ma M, Liu X and Lee KY 2020 Maximum power point tracking and voltage regulation of two-stage grid-tied PV system based on model predictive control. *Energies* 13(6). https://doi.org/10.3390/en13061304

Muhammad R, Kumar N and Kulkarni AR 2014 Power electronics : devices, circuits and applications (Fourth Edi). Pearson.

Mwinyiwiwa BMM 2016 DC Bus Voltage Regulator for Renewable Energy Based Microgrid Application. http://repository.costech.or.tz//handle/123456789/2606

Nathan K, Ghosh S, Siwakoti Y and Long T 2019 A New DC–DC Converter for Photovoltaic Systems: Coupled-Inductors Combined Cuk-SEPIC Converter. *IEEE Trans. Energy Conv*. 34(1): 191–201.
https://doi.org/10.1109/TEC.2018.2876454

Ogata K 2010 Modern control engineering. Prentice-Hall.

Ozkan Z and Hava AM 2012 A survey and extension of high efficiency grid connected transformerless solar inverters with focus on leakage current characteristics. *2012 IEEE Energy Convers. Congr. Expo. ECCE 2012*, 3453–3460. https://doi.org/10.1109/ECCE.2012.6342322

Park KB, Moon GW and Youn MJ 2012 High step-up boost converter integrated with a transformer-assisted auxiliary circuit employing quasi-resonant operation. *IEEE Trans. Power Electron. 27*(4): 1974–1984. https://doi.org/10.1109/TPEL.2011.2170223

Pradhan A and Panda B 2018 Design of DC-DC converter for load matching in case of PV system. *2017 International Conference on Energy, Communication, Data Analytics and Soft Computing, ICECDS 2017*, 1002–1007. https://doi.org/10.1109/ICECDS.2017.8389588

Rabiaa O, Mouna BH, Lassaad S, Aymen F and Aicha A 2019 Cascade Control Loop of DC-DC Boost Converter Using PI Controller. *International Symposium on Advanced Electrical and Communication Technologies, ISAECT 2018 - Proceedings*. https://doi.org/10.1109/ISAECT.2018.8618859

Shen JZ, Xiong Y, Cheng X, Fu Y and Kumar P 2006 Power MOSFET switching loss analysis: A new insight. *Conference Record - IAS Annual Meeting (IEEE Industry Applications Society)*, *3*, 1438–1442. https://doi.org/10.1109/IAS.2006.256719

Taghvaee MH, Radzi MAM, Moosavain S M, Hizam H and Hamiruce Marhaban M 2013 A current and future study on non-isolated DC–DC converters for photovoltaic applications. *Renew. Sustain. Energy Rev*. 17: 216–227. https://doi.org/10.1016/J.RSER.2012.09.023

Torkan A and Ehsani M 2018 A Novel Nonisolated Z-Source DC-DC Converter for Photovoltaic Applications. *IEEE Trans. Indusstry Appl.* 54(5): 4574–4583. https://doi.org/10.1109/TIA.2018.2833821

Vekhande V and Fernandes BG 2012 Module integrated DC-DC converter for integration of photovoltaic source with DC micro-grid. *IECON 2012 - 38th Ann. Conf. IEEE Industr. Electron. Soc.* 5657–5662. https://doi.org/10.1109/IECON.2012.6389061

Zhang L, Sun K, Xing Y, Feng L and Ge H 2011 A modular grid-connected photovoltaic generation system based on DC bus. *IEEE Trans. Power Electron.* 26(2), 523–531. https://doi.org/10.1109/TPEL.2010.2064337